THE JOURNAL OF PHYSICAL CHEMISTRY Letters

Letter

Cite This: J. Phys. Chem. Lett. 2019, 10, 2849−2856

pubs.acs.org/JPCL

Accurate Investigation on the Fluorescence Resonance Energy Transfer between Single Organic Molecules and Monolayer WSe_2 by Quantum Coherent Modulation-Enhanced Single-Molecule Imaging Microscopy

Haitao Zhou, Chengbing Qin,* Ruiyun Chen, Wenjin Zhou, Guofeng Zhang, Yan Gao, Liantuan Xiao,* and Suotang Jia

State Key Laboratory of Quantum Optics and Quantum Optics Devices, Institute of Laser Spectroscopy, Shanxi University, Taiyuan, Shanxi 030006, China

Collaborative Innovation Center of Extreme Optics, Shanxi University, Taiyuan, Shanxi 030006, China

Supporting Information

ABSTRACT: Hybrid organic two-dimensional (2D) materials heterostructures are attracting tremendous attention for optoelectronic applications due to their low-cost processing and complementary advantages. However, accurate understanding of the fundamental physics on the interface of the hybrid heterostructures at the single-molecule level remains largely unexplored. Here, we investigated the fluorescence resonance energy transfer (FRET) between the single organic molecules and monolayer WSe_2 through a newly developed single molecule microscopy technique, quantum coherent modulation-enhanced single-molecule imaging microscopy (QCME-SMIM). It is shown that the extremely weak energy transfer signal was successfully extracted from the huge fluorescence background, originating from the emission of monolayer WSe_2. The observed energy transfer efficiency is in agreement with a d^{-4} distance dependence, with a Förster radius of ∼6 nm for the hybrid structures. Our work not only provides valuable insight into the FRET process at the single-molecule level across such hybrid organic-2D interfaces, but also demonstrates the feasibility of the newly developed technique for investigating the fundamental physics of electron transfer kinetics.

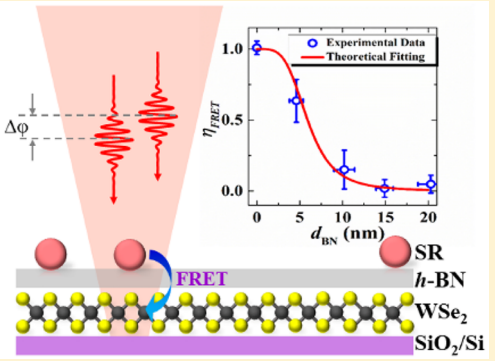

A great deal of interest has been generated recently for the emerging field of flexible optoelectronic devices based on hybrid organic−inorganic heterostructures, due to their complementary advantages.[1,2] The superior characteristics, such as thermal independence, lightweight, flexibility and high fluorescence quantum yield of organic materials,[3−5] make them particular suitable for photoelectric conversion materials.[6,7] Organic semiconductors have poor charge mobility due to their high-exciton-binding energies with covalent or ionic bands, whereas the traditional inorganic semiconductors just make up for their deficiency.[8,9] Therefore, the great advantages that benefit from pairing these disparate systems have attracted wide attention in recent decades. Organic−inorganic hybrid structures inherit the advantages of both and complements each other's insufficient, making them the next generation of highly promising photovoltaic materials based on electron transfer kinetics.[10−12]

Among the booming hybrid materials, the organic dyes−transition metal dichalcogenides (TMDCs, such as MoS_2, WS_2, and WSe_2) hybrid heterostructures have been the most strikingly highlighted, due to their two-dimensional (2D) atomic layered crystals and thus unique optical and electronic properties.[13,14] Due to the relatively large capture cross section, the integration of organic dyes with 2D materials overcomes the limited light−matter interaction in the atomic-thick layer, and greatly improves the performance of these 2D materials based optoelectronic devices.[15] Yu and co-workers first fabricated rhodamine 6G (R6G) dye-sensitized MoS_2 photodetectors, which extended the photodetection response from the band gap of MoS_2 (∼681 nm) to the infrared region (∼980 nm) with a maximum photoresponsivity of 1.17 A/W, and a total effective quantum efficiency of 280%.[16] Combining the j-aggregates of organic dyes and monolayer 2D materials, the Deotare group reported that the hybrid photodetector presented nearly 93% enhancement of photoresponsivity, due to the energy transfer from organic dyes to 2D materials.[10] Furthermore, abundant progresses have been made on 2D materials based composites as efficient counter electrodes for dye-sensitized solar cells, which can be found in recently reviews.[17,18] Despite many excellent hybrid structures have been made, the studies to understand fundamental physical

Received: March 25, 2019
Accepted: May 14, 2019
Published: May 14, 2019

DOI: 10.1021/acs.jpclett.9b00854
J. Phys. Chem. Lett. 2019, 10, 2849−2856

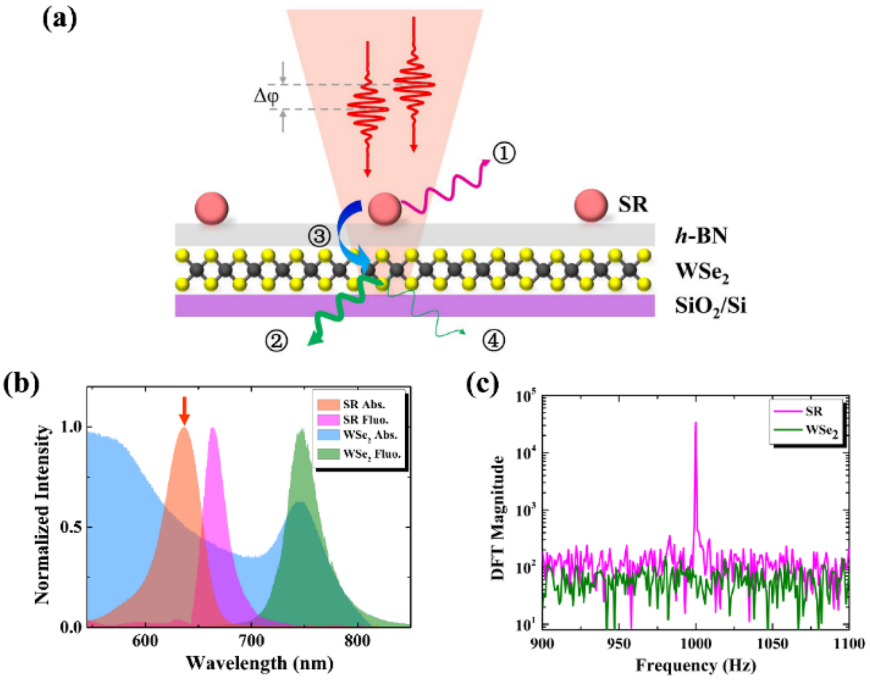

Figure 1. (a) Schematic of SR-WSe_2 structure (not to scale). An ultrashort pulse pair with a tunable phase ($\Delta\varphi$) is used to excite both the SR molecules and monolayer WSe_2. ① and ② indicate the fluorescence emission from the SR molecule and intrinsic monolayer WSe_2, respectively. ③ indicates the fluorescence resonance energy transfer (FRET) from the SR molecule to monolayer WSe_2, resulting in the photon emission of FRET process ④. (b) Normalized absorption and fluorescence spectra of SR molecules and monolayer WSe_2. The red arrow indicates the excitation laser with the wavelength of 635 nm. (c) Demodulation spectra of the arrival time of the photon series from a single SR molecule and monolayer WSe_2, respectively. The modulation frequency is 1 kHz.

processes on the interface of organic dyes−2D materials hybrid structures are still limited. These processes, including charge transfer and fluorescence resonance energy transfer (FRET),[19−22] will govern the response of the hybrid structures.[23] Traditional methods, such as time-resolved fluorescence spectra[19] and Raman spectra,[21] can be used to investigate these processes, whereas the strong and distinct signal are always required. Therefore, investigations on these processes, especially on the single-molecule level, is still a challenge, because the energy transfer signal would submerge in the background fluorescence interference of 2D materials themselves.

In this work, we reported on the study of FRET process between a single organic molecule and 2D materials (monolayer WSe_2) by using our newly developed single molecule microscopy technique, quantum coherent modulation-enhanced single-molecule imaging microscopy (QCME-SMIM).[24] This technique can effectively extract the weak signal of a single organic molecule from a huge fluorescence interference. By using QCME-SMIM, the extremely weak energy transfer signal between single organic molecules and monolayer WSe_2 has been determined. The distance dependence energy transfer efficiency has also been investigated by varying the distance between organic molecules and monolayer WSe_2 through inserting transparent medium with different thicknesses.

Here the dye molecules of squaraine-derived rotaxanes (SR, Molecular Targeting Technologies, Inc.) and monolayer WSe_2 (Shenzhen Sixcarbon Technology Co. Ltd.) were chosen as the model to investigate the FRET process, respectively owing to their relatively high quantum yields as well as separated fluorescence spectra, as shown in Figure 1b. SR molecules will act as the donor, and monolayer WSe_2 will act as the acceptor. The energy transferred from SR to WSe_2 will result in the excitation and fluorescence emission of monolayer WSe_2. While, to investigate the influences of physical variables (such as the distance and the orientation) on the FRET process, the absorption spectra as well as their fluorescence emission of the FRET pair are typical separate from each other, such as Cy3-Cy5[25] and mClover3-mRuby3.[26] In the case, one can clearly distinguish the fluorescence spectra from each of the FRET pair and determine their emission properties, by only exciting the donor. However, due to the broad absorption bands of TMDCs, as shown in Figure 1b, the laser will excite the donor (SR) and acceptor (WSe_2) simultaneously. Furthermore, the quantum yields of monolayer WSe_2 are typical in the region of 0.03% to 3%.[27,28] Despite this, due to the multielectron system of monolayer WSe_2 (i.e., vast electrons and holes in the excitation volume will recombine and emit plenty of photons at a time, in contrast, no more than one photon will emit from a single molecule at a time), its fluorescence intensity is still much stronger than that of a single SR molecule under identical excitation. Consequently, the photons originating from the FRET process are completely inundated by the intrinsic fluorescence emission of monolayer WSe_2 itself (see Supporting Information section S1 for a rough estimation of the ratio between these two branches), which hinders the investigation and elaboration of the FRET process between organic molecules and layered TMDCs.

QCME-SMIM can effectively extract weak emission of a single molecule from a huge fluorescence interference.[24] Briefly, this technique applies to the single quantum system with the two-level approximation, such as a single organic molecule and that linked with biomacromolecules. In the case,

DOI: 10.1021/acs.jpclett.9b00854
J. Phys. Chem. Lett. 2019, 10, 2849−2856

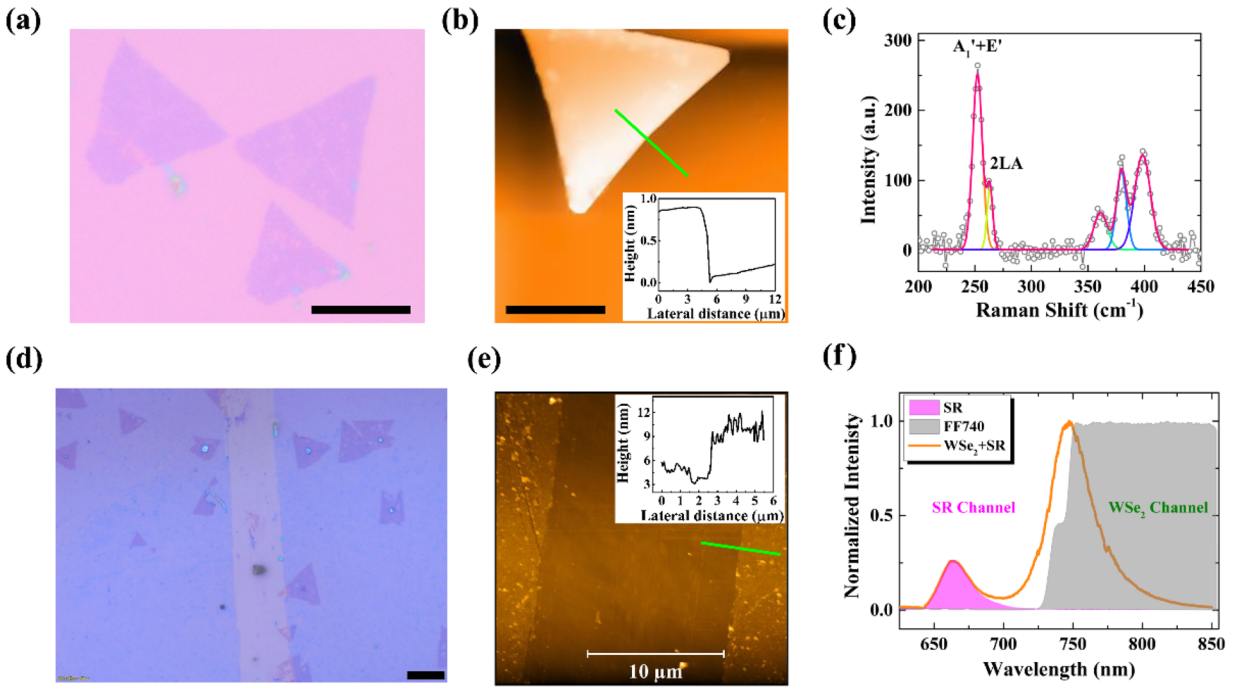

Figure 2. Characterizations of prepared samples. Optical image (a) and AFM image (b) of WSe_2 prepared by chemical vapor deposition. The inset is the height profile of the selected line. Scale bar: 10 μm. (c) Raman spectra of monolayer WSe_2. Optical image (d) and AFM (e) of WSe_2 flakes encapsulated with *h*-BN film. To show the presence of *h*-BN, a striation made on the film is evidence as a light strip. Scale bar: 10 μm. The inset is the height profile of the selected line. (f) Fluorescence spectrum of a single SR molecule-monolayer WSe_2 hybrid material. The pink color denotes the fluorescence spectrum of condense SR molecules, the gray color denotes the transmission spectrum of the FF740 filter. The fluorescence reflected by the FF740 is labeled as the SR channel, and that transmitted by the FF740 is labeled as the WSe_2 channel.

a coherent state of the single molecule can be prepared by an ultrashort pulse pair.[29] By periodically modulating the phase difference between the ultrashort pulses pair, the excited-state population probability of the single molecule can be availably modulated, which results in the modulation of its fluorescence emission. Thus, the weak signal from the single molecule can be flexibly determined by demodulating its photon series through discrete Fourier transform (DFT) at modulation frequency, as the pink curve shown in Figure 1c (see Supporting Information section S3 for the detail of data processing). While for the other systems, such as TMDCs semiconductor materials, their excited state population probabilities cannot be varied correspondingly to the modulation of phase difference (Figure S6 in the Supporting Information). Hence, their fluorescence emission will remain at the same value, and no obvious demodulation signal can be determined at modulation frequency, as the green curve shown in Figure 1c. However, the emitted photons of the acceptor (monolayer WSe_2) arising from the FRET process still have a modulation effect, and thus the corresponding signal can still be digged out by QCME-SMIM. Here, we propose a scheme to investigate the FRET process between single SR molecules and monolayer WSe_2, as illustrated in Figure 1a. A pair of ultrashort pulse laser with tunable phase difference is used to excite single SR molecules (see Supporting Information section S2 for the detailed experimental setup and the relevant parameters). By collecting the emission from the spectra region of monolayer WSe_2 and performing DFT, we can extract the signal from the FRET process and investigate the influences of physical variables on their interaction.

In the experiment, WSe_2 was first grown on a sapphire substrate by using the conventional chemical vapor deposition (CVD) method and then transferred to a SiO_2/Si substrate with a poly(methyl methacrylate) (PMMA) assisted method.[30] Figure 2a shows an optical image of a typical sample. Isolated flakes with triangular shape and edge lengths ranging from 10 to 20 μm can be clearly observed. Meanwhile, we can also clearly see many defects on top of the triangular flakes, such as holes, residual reagents, and secondary nucleation sites.[31,32] These defects will lead to the nonuniform fluorescence emission, as will be discussed later. The thicknesses of these WSe_2 flakes have been explored by atomic force microscopy (AFM) characterization, as shown in Figure 2b. The relatively homogeneous color contrast in the AFM image indicates that the basal plane of the WSe_2 flake is flat and uniform. The thickness of ~0.8 nm confirms that the flake is a monolayer. Raman spectroscopy was also employed to further characterize these triangular flakes. According to the previous works,[33−35] the strong peak around 250 cm^{-1} can be attributed to the combination of two first-order Raman modes with A' and E' symmetries, and the shoulder peak can be assigned to the overtone of the longitudinal acoustic (LA) phonon branch. A group of three peaks in the region of 350−425 cm^{-1} is not fully understood; however, a preliminary assignment can be found in refs 34 and 35.

To study the distance dependence of FRET in SR-WSe_2 system and prevent Dexter transfer between the two materials, a transparent medium of hexagonal boron nitride (*h*-BN) film was inserted between SR molecules and WSe_2. The *h*-BN was first synthesized on Cu substrate using CVD method with two heating zones under low pressure,[36] and then transferred and covered on top of monolayer WSe_2 by Cu etching method with the assist of PMMA.[37] Figure 2d presents the optical image of a prepared WSe_2/*h*-BN sample, where a striation was prepared.

DOI: 10.1021/acs.jpclett.9b00854
J. Phys. Chem. Lett. 2019, 10, 2849−2856

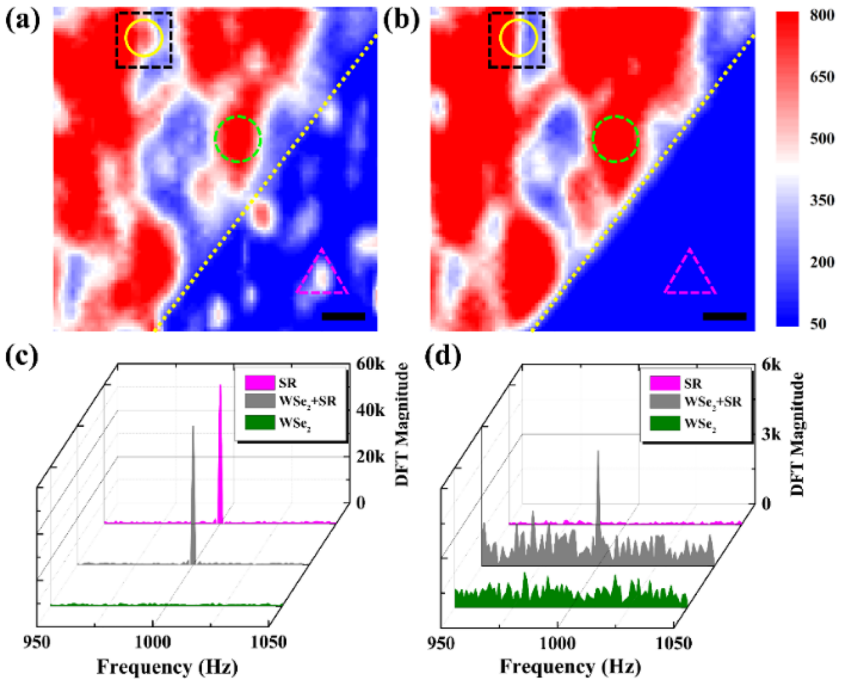

Figure 3. Traditional fluorescence intensity imaging and demodulation spectra of SR-WSe_2 hybrid materials. (a) and (b) are the fluorescence intensity images of the SR and WSe_2 channels, respectively, with the integration time of 0.1 s for each pixel. The images are divided into two parts by the yellow dotted line, the upper left part is the images of hybrid materials, while the lower right part is the images of SR molecules. The dashed triangle, circle, and square indicate the fluorescence emission from a single SR molecule, intrinsic monolayer WSe_2, and the hybrid materials, respectively. The solid circle indicates the presence of a SR molecule. Scale bar: 1 μm. (c) and (d) show the demodulation spectra of the three marked areas for SR and WSe_2 channels with integration time 50 s, respectively.

As a consequence, the presence of *h*-BN and the corresponding thickness (d_{BN}) can be readily determined. From the AFM and the height profile shown in Figure 2e, the thickness of the *h*-BN film is about 4.6 nm. Then, SR molecules were spin-coated onto the *h*-BN films. By carefully controlling the concentration of SR solution and the spin coating parameters, individual SR molecules can be well separated with each other. Figure 2f displays the fluorescence spectra of the SR-WSe_2 hybrid materials (with the thickness of intermediate *h*-BN to be ~4.6 nm). It can be found that the fluorescence intensity of monolayer WSe_2 is about 5-fold stronger than that of a single SR molecule. To completely eliminate the influence of intrinsic fluorescence emission from SR molecules to the FRET process, we divided the fluorescence of hybrid materials into two parts by a FF740 dichroic mirror (Semrock), as highlighted by the gray dashed line in Figure 2f. The short wavelength part records the emission from SR and partial fluorescence of WSe_2 shorter than 740 nm (as well as partial FRET photons). For the sake of simplicity, we named this region as the SR channel hereinafter for short. While the long wavelength part takes the photons from intrinsic monolayer WSe_2 as well as the FRET process, which is named as the WSe_2 channel hereinafter for short.

Prior to FRET investigation, we first performed the fluorescence intensity images of the hybrid sample. Figure 3a and 3b are the traditional fluorescence images of the same area for the SR and WSe_2 channels, respectively. The upper left part is the hybrid area, while the patterns in the lower right part are all from SR molecules. The boundary between them has been highlighted by a yellow dashed line. Obviously, patterns of molecules can only be observed in the SR channel, which is in good agreement with its spectra and the filter we used, as shown in Figure 2f. Most of these patterns have been proved to be the emission from single SR molecules, by measuring their second order correlation function (see Supporting Information section S4 for the definition of a single molecule and the control sample that SR molecules was spin-coating on bare *h*-BN film). Thus, we can believe that SR molecules in the hybrid area are also separated with each other well. By demodulating the fluorescence photon series from a single molecule (such as the pattern marked with a triangle) through DFT, it manifests a large magnitude in the SR channel, as shown in Figure 3c. This result is consisting with our previous work.[24] On the other aspect, fluorescence emission from monolayer WSe_2 can be observed in both channels, which present inhomogeneous patterns. This anisotropy mainly results from the abundant defects on the surface of WSe_2, as we found in the optical image. In the hybrid areas, most of the patterns only originate from the intrinsic emission of monolayer WSe_2, as highlighted by a dashed circle. These patterns display no demodulation signal in either channel (the green curves shown in Figure 3c and d), in accord with Figure 1c. While, some patterns present large DFT magnitudes in the SR channel, as marked by the dashed square (see Supporting Information section S5 for the demodulation imaging). More importantly, they present substantial magnitudes in the WSe_2 channel simultaneously, as the black curves shown in Figure 3c and d. By comparing and carefully checking the two channels, we still can find the indicator of the single molecule in the SR channel, as highlighted by the solid circle. However, the corresponding pattern from FRET process completely vanished in the WSe_2 channel, due to the low quantum yield of WSe_2 but their strong intrinsic fluorescence emission. While, the emerging of a DFT magnitude confirms the presence of FRET process

DOI: 10.1021/acs.jpclett.9b00854
J. Phys. Chem. Lett. 2019, 10, 2849−2856

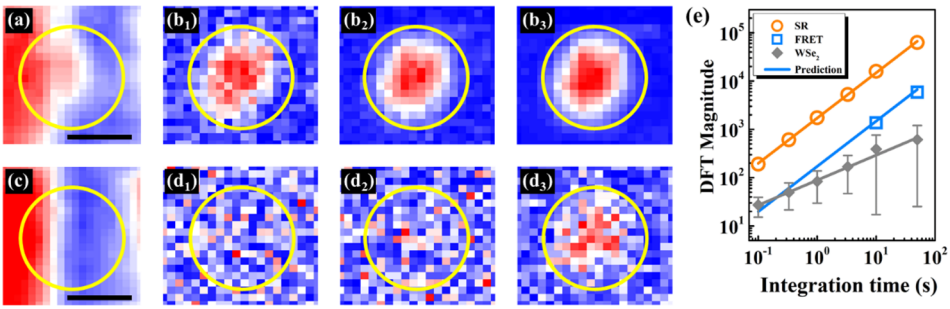

Figure 4. Fluorescence intensity imaging and demodulation imaging. (a) and (c) are the fluorescence intensity images of the SR and WSe_2 channels for the square area marked in Figure 3, respectively. Scale bar: 1 μm. (b_1), (b_2), and (b_3) show the demodulation imaging of (a) with integration time 0.1, 1, and 10 s, respectively. (d_1), (d_2) and (d_3) are the demodulation imaging of (c) with integration time 0.1, 1, and 10 s, respectively. (e) DFT magnitudes as a function of integration time. The orange circles, hollow squares and solid diamonds denote DFT magnitudes of the emission from the SR molecule, the FRET process, and the intrinsic monolayer WSe_2. The origin solid line is the linear fitting of the experiment data and the correlation coefficients (R^2) is 0.9994. The gray solid line is the power fitting ($y = ax^b$). R^2 and b are 0.976 and 0.518, respectively. The blue solid line is the theoretical prediction.

between the single SR molecule and monolayer WSe_2 (The presence of FRET has also been proven by the quenching of demodulation magnitude of SR molecules. See Supporting Information section S7 for details). In other words, the modulation of the single molecules have been transferred to the emission of monolayer WSe_2 by the FRET process.

The presence of FRET between SR and WSe_2 can be further confirmed by the demodulation imaging, which can be obtained by conducting DFT on each pixel and extracting the demodulation magnitudes. Figure 4a and 4c are the traditional fluorescence intensity imaging of the SR and WSe_2 channels for the square area shown in Figure 3, respectively. Figure 4b and d shows the demodulation imaging of the two channels for the same area with the integration time of 0.1, 1, and 10 s, respectively. The pattern originating from the single SR molecule has been highlighted by the dashed circles. For the SR channel, the signal is gradually enhanced as the increasing of the integration time. The signal as a function of integration time can be well fitted by a linear relationship, consisting with theoretical prediction and previous experimental results.[24] While for the WSe_2 channel, the signal originating from the FRET process cannot be determined in a short integration time, because very few photons from the FRET have been collected and demodulated. Thus, the DFT magnitude of FRET photons is comparable or even smaller than that of intrinsic WSe_2 emission, as shown in Figure 4d_1 and d_2. To our delight, this predicament can be overcome by increasing the integration time. According to the prediction of QCEM-SMIM, the DFT magnitude of the system without coherent property (such as WSe_2 in this experiment) only presents short noise feature, which will be increased over integration time as a power law with the exponent of 0.5. This is proved by analyzing the DFT magnitude of intrinsic WSe_2 emission as the function of the integration time, as shown in Figure 4e, where the exponent is 0.518. On the other hand, the DFT magnitude of photon series with coherent property is increasing linearly as the function of integration time, as discussed above for the DFT magnitude of the single SR molecule and our previous works. Thus, with the increasing of the integration time, the signal of FRET photons will become clear, as shown in Figure 4d_3. Furthermore, the DFT magnitude of FRET photons varied as the integration time can be predicted according to the relationship between the intensity of SR emission and FRET process, as the blue line shown in Figure 4e (see Supporting Information section S9 for the derivation). The good agreements between the experimental data (the blue hollow squares) and predicted line indicate the feasibility and applicability of our approach.

Our approach not only can prove the presence of energy transfer between organic molecules and layered TMDCs, but also can quantitatively determine the distance dependence of the energy transfer efficiency. According to the prediction of QCEM-SMIM and previous works, the DFT magnitude is proportional to the number of photons from a single molecule, thus the energy transfer efficiency, η_{FRET}, can be determined by the formula as follows:

$$\eta_{\mathrm{FRET}} = \frac{k_{\mathrm{FRET}}}{k_{\mathrm{FRET}} + k_{\mathrm{r}} + k_{\mathrm{nr}}} = \frac{(M_{\mathrm{FRET}} - N_{\mathrm{FRET}})/(\alpha Q_{\mathrm{WSe_2}})}{(M_{\mathrm{SR}} - N_{\mathrm{SR}})/Q_{\mathrm{SR}} + (M_{\mathrm{FRET}} - N_{\mathrm{FRET}})/(\alpha Q_{\mathrm{WSe_2}})} \quad (1)$$

where k_{FRET} is the FRET rate between SR and monolayer WSe_2, and k_r and k_{nr} are the radiation and nonradiation rates of SR, respectively. M_{FRET} and M_{SR} are the demodulation magnitude for the fluorescence with a single SR molecule in the WSe_2 and SR channels, and N_{FRET} and N_{SR} are the demodulation magnitude for the fluorescence without a single SR molecule in the WSe_2 and SR channels, respectively. $Q_{\mathrm{WSe_2}}$ and Q_{SR} are the quantum yield of monolayer WSe_2 and SR organic molecules. α is the ratio of the fluorescence intensity of monolayer WSe_2 in the WSe_2 channel to the full fluorescence intensity of monolayer WSe_2 to calibrate the FRET signal filtering by FF740. The detailed derivation can be found in Supporting Information section S8.

In the experiment, M_{SR}, M_{FRET}, N_{FRET}, and N_{SR} are obtained by DFT of fluorescence photons from the two channels. The DFT magnitudes of the square area shown in Figure 3 are 6.63×10^4 for the SR channel (M_{SR}) and 4.96×10^3 for the WSe_2 channel (M_{FRET}), respectively. The corresponding magnitudes for N_{FRET} and N_{SR} are 799.7 and 419.4, respectively. Q_{SR} of the SR solution was measured to be 0.58.[38] On the other side, $Q_{\mathrm{WSe_2}}$ of monolayer WSe_2 has a broad distribution (see Supporting Information section S11 for the histogram of $Q_{\mathrm{WSe_2}}$), due to the presence of many defects. Here, we used the averaged value of 5.05% (see Supporting Information sections S10 and S11 for the calibration of the collection efficiency of

DOI: 10.1021/acs.jpclett.9b00854
J. Phys. Chem. Lett. 2019, 10, 2849−2856

our system and the determination of Q_{WSe_2}). α can be obtained by calculating the ratio of the spectrum of WSe_2 in two channels through Figure 2f, equaling to 0.72. Thus, the efficiency of energy transfer, η_{FRET} = 0.50, can be determined.

To reduce the influence of anisotropic optical properties on the FRET efficiency, including the relative transition dipole moment orientations between single molecules and 2D materials and the nonuniform fluorescence intensity of monolayer WSe_2, the efficiencies of more than 100 single SR molecules on a certain *h*-BN thickness have been investigated. Figure 5a presents the distributions of energy transfer

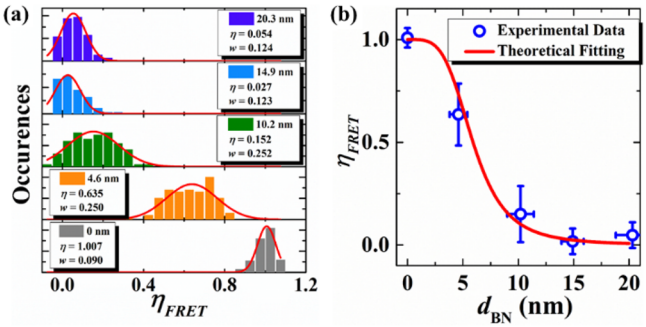

Figure 5. (a) Distributions of energy transfer efficiency, η_{FRET}, under different *h*-BN thicknesses. The solid lines are the Gauss fitting. (b) Plot of the energy transfer efficiency as a function of the thickness of the thickness of the *h*-BN. The experimental data and the corresponding error bars are derived from the Gauss fitting.

efficiency under different *h*-BN thicknesses. The full width at half-maximum (fwhm) of these distributions are pretty broad, which can be attributed to the inhomogeneous quality of monolayer WSe_2. The narrow distribution is expected for a preparation of high-quality WSe_2. According to the point-to-face energy transfer relationship, expressed as[23,39−41]

$$\eta_{FRET} = \left(1 + \left(\frac{r}{R}\right)^4\right)^{-1} \quad (2)$$

where r is the distance between the donor and acceptor. In other words, r is the thickness of *h*-BN film in this experiment, i.e., d_{BN}. R is the Förster distance at which the energy transfer efficiency is 0.5 (see Supporting Information section S12 for the derivation and the relevant assumptions). Fitting the experiment data by eq 2, as shown in Figure 5b, R is determined to be 5.9 nm.

The broad distribution of energy transfer efficiency is mainly due to the defect of monolayer WSe_2, which stems from the nanometer detection sensitivity of single molecules. Whereas, the traditional methods usually get the energy transfer efficiency at the ensemble level. They average the effects of nanoscale defects, which are crucial for the properties of 2D material based devices. The QCME-SMIM method based on single molecule microscopy can eliminate the ensemble average effect. Thus, our approach is of guiding significance for studying the energy transfer of hybrid materials at the nanoscale.

In conclusion, we investigated the FRET process between single SR molecules and monolayer WSe_2 by QCME-SMIM. The faint signal of FRET process drowning in the huge WSe_2 fluorescence interference can be extracted by modem technology based on the different quantum coherent properties between SR molecules and monolayer WSe_2. By measuring the DFT magnitude of the SR emission and FRET photons, we demonstrated the energy transfer efficiency of the SR-WSe_2 hybrid structures. Furthermore, by inserting the transparent *h*-BN with different thicknesses between SR molecules and monolayer WSe_2, a Förster radius of 5.9 nm was clearly determined. Such a long FRET distance might originate from the quantum coherence property of organic molecules,[42,43] which increases the distance of energy transfer and can potentially improve the performance of photoelectric device. In addition, the QCME-SMIM method based on single molecule microscopy can eliminate the ensemble average effect, and it can be used to study the impact of defect on the electron transfer kinetics of hybrid materials at the nanoscale.

■ ASSOCIATED CONTENT

Supporting Information

The Supporting Information is available free of charge on the ACS Publications website at DOI: 10.1021/acs.jpclett.9b00854.

Estimation of the branch ratio of FRET; experimental setup; data processing; sample preparation; definition of the single molecule; comparing the fluorescence imaging and demodulation imaging; comparing the modulation of WSe_2 and SR fluorescence trajectories; derivation of FRET efficiency; calibration of the collection efficiency; measurement of the quantum yield of monolayer WSe_2 (PDF)

■ AUTHOR INFORMATION

Corresponding Authors

*E-mail: chbqin@sxu.edu.cn (C.Q.).
*E-mail: xlt@sxu.edu.cn (L.X.).

ORCID

Haitao Zhou: 0000-0001-5325-5275
Chengbing Qin: 0000-0002-6822-5113
Guofeng Zhang: 0000-0002-9030-0431
Liantuan Xiao: 0000-0003-2690-6460

Notes

The authors declare no competing financial interest.

■ ACKNOWLEDGMENTS

The authors gratefully acknowledge support from the National Key Research and Development Program of China (Grant No. 2017YFA0304203), National Natural Science Foundation of China (Grant No. 11434007), Natural Science Foundation of China (Nos. 61875109, 61527824, 61675119, 11504216, and 61605104), PCSIRT (No. IRT_17R70), 1331KSC, 111 project (Grant No. D18001) and STIP (No. 201802019).

■ REFERENCES

(1) Kaushik, A.; Kumar, R.; Arya, S. K.; Nair, M.; Malhotra, B. D.; Bhansali, S. Organic-Inorganic Hybrid Nanocomposite-Based Gas Sensors for Environmental Monitoring. *Chem. Rev.* **2015**, *115*, 4571−4606.

(2) Braga, D.; Grepioni, F.; Shemchuk, O. Organic-Inorganic Ionic Co-Crystals: A New Class of Multipurpose Compounds. *CrystEngComm* **2018**, *20*, 2212−2220.

(3) Azzellino, G.; Grimoldi, A.; Binda, M.; Caironi, M.; Natali, D.; Sampietro, M. Fully Inkjet-Printed Organic Photodetectors with High Quantum Yield. *Adv. Mater.* **2013**, *25*, 6829−6833.

DOI: 10.1021/acs.jpclett.9b00854
J. Phys. Chem. Lett. 2019, 10, 2849−2856

(4) Goetz, K. P.; Fonari, A.; Vermeulen, D.; Hu, P.; Jiang, H.; Diemer, P. J.; Ward, J. W.; Payne, M. E.; Day, C. S.; Kloc, C.; et al. Freezing-in Orientational Disorder Induces Crossover from Thermally-Activated to Temperature-Independent Transport in Organic Semiconductors. *Nat. Commun.* **2014**, *5*, 5642.
(5) Kaltenbrunner, M.; White, M. S.; Glowacki, E. D.; Sekitani, T.; Someya, T.; Sariciftci, N. S.; Bauer, S. Ultrathin and Lightweight Organic Solar Cells with High Flexibility. *Nat. Commun.* **2012**, *3*, 770.
(6) Zhang, J.; Xu, W.; Sheng, P.; Zhao, G.; Zhu, D. Organic Donor-Acceptor Complexes as Novel Organic Semiconductors. *Acc. Chem. Res.* **2017**, *50*, 1654−1662.
(7) Zhao, F.; Wang, C.; Zhan, X. Morphology Control in Organic Solar Cells. *Adv. Energy Mater.* **2018**, *8*, 1703147.
(8) Kang, S. D.; Snyder, G. J. Charge-Transport Model for Conducting Polymers. *Nat. Mater.* **2017**, *16*, 252−257.
(9) Smits, E. C. P.; Mathijssen, S. G. J.; van Hal, P. A.; Setayesh, S.; Geuns, T. C. T.; Mutsaers, K. A. H. A.; Cantatore, E.; Wondergem, H. J.; Werzer, O.; Resel, R.; et al. Bottom-up Organic Integrated Circuits. *Nature* **2008**, *455*, 956−959.
(10) Cheng, C.-H.; Li, Z.; Hambarde, A.; Deotare, P. B. Efficient Energy Transfer across Organic-2D Inorganic Heterointerfaces. *ACS Appl. Mater. Interfaces* **2018**, *10*, 39336−39342.
(11) Hoque, M. N. F.; He, R.; Warzywoda, J.; Fan, Z. Effects of Moisture-Based Grain Boundary Passivation on Cell Performance and Ionic Migration in Organic-Inorganic Halide Perovskite Solar Cells. *ACS Appl. Mater. Interfaces* **2018**, *10*, 30322−30329.
(12) Pan, Z.; Yao, L.; Zhai, J.; Yao, X.; Chen, H. Interfacial Coupling Effect in Organic/Inorganic Nanocomposites with High Energy Density. *Adv. Mater.* **2018**, *30*, 1705662.
(13) Duan, X.; Wang, C.; Pan, A.; Yu, R.; Duan, X. Two-Dimensional Transition Metal Dichalcogenides as Atomically Thin Semiconductors: Opportunities and Challenges. *Chem. Soc. Rev.* **2015**, *44*, 8859−8876.
(14) Wang, Q. H.; Kalantar-Zadeh, K.; Kis, A.; Coleman, J. N.; Strano, M. S. Electronics and Optoelectronics of Two-Dimensional Transition Metal Dichalcogenides. *Nat. Nanotechnol.* **2012**, *7*, 699−712.
(15) Jariwala, D.; Howell, S. L.; Chen, K.-S.; Kang, J.; Sangwan, V. K.; Filippone, S. A.; Turrisi, R.; Marks, T. J.; Lauhon, L. J.; Hersam, M. C. Hybrid, Gate-Tunable, Van Der Waals P-N Heterojunctions from Pentacene and MoS_2. *Nano Lett.* **2016**, *16*, 497−503.
(16) Yu, S. H.; Lee, Y.; Jang, S. K.; Kang, J.; Jeon, J.; Lee, C.; Lee, J. Y.; Kim, H.; Hwang, E.; Lee, S.; et al. Dye-Sensitized MoS_2 Photodetector with Enhanced Spectral Photoresponse. *ACS Nano* **2014**, *8*, 8285−8291.
(17) Gobbi, M.; Orgiu, E.; Samori, P. When 2D Materials Meet Molecules: Opportunities and Challenges of Hybrid Organic/Inorganic Van Der Waals Heterostructures. *Adv. Mater.* **2018**, *30*, No. e1706103.
(18) Huang, Y. L.; Zheng, Y. J.; Song, Z.; Chi, D.; Wee, A. T. S.; Quek, S. Y. The Organic-2D Transition Metal Dichalcogenide Heterointerface. *Chem. Soc. Rev.* **2018**, *47*, 3241−3264.
(19) Zang, H.; Routh, P. K.; Huang, Y.; Chen, J. S.; Sutter, E.; Sutter, P.; Cotlet, M. Nonradiative Energy Transfer from Individual CdSe/ZnS Quantum Dots to Single-Layer and Few-Layer Tin Disulfide. *ACS Nano* **2016**, *10*, 4790−4796.
(20) Sampat, S.; Guo, T.; Zhang, K.; Robinson, J. A.; Ghosh, Y.; Acharya, K. P.; Htoon, H.; Hollingsworth, J. A.; Gartstein, Y. N.; Malko, A. V. Exciton and Trion Energy Transfer from Giant Semiconductor Nanocrystals to MoS_2 Monolayers. *ACS Photonics* **2016**, *3*, 708−715.
(21) Roy, S.; Neupane, G. P.; Dhakal, K. P.; Lee, J.; Yun, S. J.; Han, G. H.; Kim, J. Observation of Charge Transfer in Heterostructures Composed of $MoSe_2$ Quantum Dots and a Monolayer of MoS_2 or WSe_2. *J. Phys. Chem. C* **2017**, *121*, 1997−2004.
(22) Raja, A.; Montoya Castillo, A.; Zultak, J.; Zhang, X. X.; Ye, Z.; Roquelet, C.; Chenet, D. A.; van der Zande, A. M.; Huang, P.; Jockusch, S.; et al. Energy Transfer from Quantum Dots to Graphene and MoS_2: The Role of Absorption and Screening in Two-Dimensional Materials. *Nano Lett.* **2016**, *16*, 2328−2333.
(23) Federspiel, F.; Froehlicher, G.; Nasilowski, M.; Pedetti, S.; Mahmood, A.; Doudin, B.; Park, S.; Lee, J. O.; Halley, D.; Dubertret, B.; et al. Distance Dependence of the Energy Transfer Rate from a Single Semiconductor Nanostructure to Graphene. *Nano Lett.* **2015**, *15*, 1252−1258.
(24) Zhou, H.; Qin, C.; Chen, R.; Liu, Y.; Zhou, W.; Zhang, G.; Gao, Y.; Xiao, L.; Jia, S. Quantum Coherent Modulation-Enhanced Single-Molecule Imaging Microscopy. *J. Phys. Chem. Lett.* **2019**, *10*, 223−228.
(25) Ishikawa-Ankerhold, H. C.; Ankerhold, R.; Drummen, G. P. Advanced Fluorescence Microscopy Techniques—Frap, Flip, Flap, Fret and Flim. *Molecules* **2012**, *17*, 4047−4132.
(26) Bajar, B.; Wang, E.; Zhang, S.; Lin, M.; Chu, J. A Guide to Fluorescent Protein Fret Pairs. *Sensors* **2016**, *16*, 1488.
(27) Mohamed, N. B.; Wang, F.; Lim, H. E.; Zhang, W.; Koirala, S.; Mouri, S.; Miyauchi, Y.; Matsuda, K. Evaluation of Photoluminescence Quantum Yield of Monolayer WSe_2 Using Reference Dye of 3-Borylbithiophene Derivative. *Phys. Status Solidi B* **2017**, *254*, 1600563.
(28) Kim, H.; Ahn, G. H.; Cho, J.; Amani, M.; Mastandrea, J. P.; Groschner, C. K.; Lien, D. H.; Zhao, Y. B.; Ager, J. W.; Scott, M. C.; et al. Synthetic WSe_2 Monolayers with High Photoluminescence Quantum Yield. *Sci. Adv.* **2019**, *5*, No. eaau4728.
(29) Hildner, R.; Brinks, D.; van Hulst, N. F. Femtosecond Coherence and Quantum Control of Single Molecules at Room Temperature. *Nat. Phys.* **2011**, *7*, 172−177.
(30) Yin, J.; Li, J.; Chen, H.; Wang, J.; Yan, P.; Liu, M.; Liu, W.; Lu, W.; Xu, Z.; Zhang, W.; et al. Large-Area Highly Crystalline Wse_2 Atomic Layers for Ultrafast Pulsed Lasers. *Opt. Express* **2017**, *25*, 30020−30031.
(31) Zhou, D.; Shu, H.; Hu, C.; Jiang, L.; Liang, P.; Chen, X. Unveiling the Growth Mechanism of MoS_2 with Chemical Vapor Deposition: From Two-Dimensional Planar Nucleation to Self-Seeding Nucleation. *Cryst. Growth Des.* **2018**, *18*, 1012−1019.
(32) Wu, D.; Min, T.; Zhou, J.; Li, C.; Ma, G.; Lu, G.; Xia, M.; Gu, Z. Effect of Substrate Symmetry on the Dendrite Morphology of MoS_2 Film Synthesized by CVD. *Sci. Rep.* **2017**, *7*, 15166.
(33) Yang, M.; Cheng, X.; Li, Y.; Ren, Y.; Liu, M.; Qi, Z. Anharmonicity of Monolayer MoS_2, $MoSe_2$, and WSe_2: A Raman Study under High Pressure and Elevated Temperature. *Appl. Phys. Lett.* **2017**, *110*, 093108.
(34) Zhao, W.; Ghorannevis, Z.; Amara, K. K.; Pang, J. R.; Toh, M.; Zhang, X.; Kloc, C.; Tan, P. H.; Eda, G. Lattice Dynamics in Mono- and Few-Layer Sheets of WS_2 and WSe_2. *Nanoscale* **2013**, *5*, 9677−9683.
(35) del Corro, E.; Terrones, H.; Elias, A.; Fantini, C.; Feng, S.; Nguyen, M. A.; Mallouk, T. E.; Terrones, M.; Pimenta, M. A. Excited Excitonic States in 1L, 2L, 3L, and Bulk WSe_2 Observed by Resonant Raman Spectroscopy. *ACS Nano* **2014**, *8*, 9629−9635.
(36) Kim, K. K.; Hsu, A.; Jia, X.; Kim, S. M.; Shi, Y.; Hofmann, M.; Nezich, D.; Rodriguez-Nieva, J. F.; Dresselhaus, M.; Palacios, T.; et al. Synthesis of Monolayer Hexagonal Boron Nitride on Cu Foil Using Chemical Vapor Deposition. *Nano Lett.* **2012**, *12*, 161−166.
(37) Van Ngoc, H.; Qian, Y.; Han, S. K.; Kang, D. J. Pmma-Etching-Free Transfer of Wafer-Scale Chemical Vapor Deposition Two-Dimensional Atomic Crystal by a Water Soluble Polyvinyl Alcohol Polymer Method. *Sci. Rep.* **2016**, *6*, 33096.
(38) Arunkumar, E.; Forbes, C. C.; Noll, B. C.; Smith, B. D. Squaraine-Derived Rotaxanes: Sterically Protected Fluorescent near-Ir Dyes. *J. Am. Chem. Soc.* **2005**, *127*, 3288−3289.
(39) Goodfellow, K. M.; Chakraborty, C.; Sowers, K.; Waduge, P.; Wanunu, M.; Krauss, T.; Driscoll, K.; Vamivakas, A. N. Distance-Dependent Energy Transfer between CdSe/CdS Quantum Dots and a Two-Dimensional Semiconductor. *Appl. Phys. Lett.* **2016**, *108*, 021101.
(40) Kuhn, H. Classical Aspects of Energy Transfer in Molecular Systems. *J. Chem. Phys.* **1970**, *53*, 101−108.

DOI: 10.1021/acs.jpclett.9b00854
J. Phys. Chem. Lett. 2019, 10, 2849−2856

(41) Chance, R.; Prock, A.; Silbey, R. Molecular Fluorescence and Energy Transfer near Interfaces. *Adv. Chem. Phys.* **2007**, *37*, 1−65.
(42) Rafiq, S.; Scholes, G. D. From Fundamental Theories to Quantum Coherences in Electron Transfer. *J. Am. Chem. Soc.* **2019**, *141*, 708−722.
(43) Brédas, J.-L.; Sargent, E. H.; Scholes, G. D. Photovoltaic Concepts Inspired by Coherence Effects in Photosynthetic Systems. *Nat. Mater.* **2017**, *16*, 35−44.

DOI: 10.1021/acs.jpclett.9b00854
J. Phys. Chem. Lett. 2019, 10, 2849−2856